Growth thermodynamics of nanowires and its application to polytypism of zinc blende III-V nanowires

V. G. Dubrovskii[1,2,*] and N. V. Sibirev[1]

[1]*St.-Petersburg Physical Technological Centre of the Russian Academy of Sciences for Research and Education, Khlopina 8/3, 195220 St.-Petersburg, Russia*

[2]*Ioffe Physical Technical Institute of the Russian Academy of Sciences, Politekhnicheskaya 26, 194021 St.-Petersburg, Russia*

(Received 8 August 2007; revised manuscript received 21 September 2007; published 15 January 2008)

Theoretical model for the growth thermodynamics of nanowires in different epitaxial techniques is presented, which enables one to determine morphological and structural configurations of the nanowire ensemble with minimum formation energy. It is demonstrated that nanowire ensembles are metastable and controlled entirely by the growth kinetics. The model is applied to studying the polytypism of zinc blende III-V nanowires. It is shown that structural transition should occur within a certain domain of radii and vapor supersaturations. Different polytypes between wurtzite and zinc blende structures with periodicity up to 18 layers are analyzed. It is demonstrated that 4*H* polytype has the lowest formation energy and the largest critical radius of transition amongst all polytypes. Numerical estimates predict the critical radius of structural phase transition of 17–25 nm for GaAs nanowires growing on the GaAs(111)*B* substrate.

DOI: 10.1103/PhysRevB.77.035414 PACS number(s): 81.10.Aj, 68.70.+w

I. INTRODUCTION

A continuously growing interest to semiconductor nanowires (NWs) ranges from potential applications as building blocks for advanced electronic,[1] photonic,[2] sensing,[3] and other functional nanodevices to fundamental aspects of NW growth[4–6] and physical properties.[7–9] Using modern epitaxial techniques, freestanding NWs with radii typically of order of tens of nanometers and lengths up to tens of micrometers can be obtained. These techniques utilize the growth on the substrates activated by catalyst drops[1–6] or catalyst-free selective area growth.[10,11] Surface arrangement and radii of NWs are dictated by the position and size of growth seeds, and the length is determined by the deposition time. It is therefore possible to produce regular arrays of NWs by organizing the surface before growth.[1–4,10] Due to very efficient lateral stress relaxation, NWs are promising for fabrication of coherent strained heterostructures[12] and dislocation-free growth on the lattice-mismatched substrates, in particular, of III-V compounds on Si, which is paramount for integration of optoelectronic and microelectronic devices.[13]

Many recent investigations[4–8,12–16] have been devoted to studying the growth mechanisms of different III-V NWs in metal organic chemical vapor deposition (MOCVD), molecular beam epitaxy (MBE), and chemical beam epitaxy (CBE) techniques. It is now generally recognized that the thermodynamic driving force for NW formation is the vapor supersaturation with respect to the solid phase, while the kinetic growth processes contributing to the growth involve surface diffusion[4,5] and nucleation.[14] Depending on the temperature and the material-catalyst combination, catalyst-assisted growth may proceed via the vapor-liquid-solid[17] (VLS) or vapor-solid-solid[8] (VSS) mechanism. In chemical epitaxies involving the precursor decomposition mechanism (MOCVD and CBE), the drop acts as a chemical catalyst inhibiting the reaction at its surface.[4,15,17] In MBE technique, the particle rather plays a role of physical catalyst, collecting the adatoms from the surface[5,15,16] and facilitating the NW growth under the drop.[14] Despite of reasonable understanding of the growth behavior, it is not completely clear so far whether the NW formation is thermodynamically or kinetically controlled. In other words, is there an energetically favorable phase and morphological configuration of the system relating to a stable NW ensemble, or it is metastable and can only be observed at the kinetic stage of growth? It is well known that the growth of epitaxial nanostructures always involves the energetically unfavorable process of formation of lateral surface.[18] Given the huge surface to volume ratio in NWs, one can initially anticipate that all NW ensembles are metastable. In this case, it is important to know the metastable configuration with minimum energy (which would be most probably observed in growth experiment) and also the domain of parameters separating metastable and unstable states (which formation should be considered as thermodynamically forbidden). In these investigations, we should take into consideration the crystallographic structure of NWs, because structural stability in NWs differs from that of the bulk form.[19,20]

Recent studies[6–9,11,13,21] demonstrate that, unlike in the bulk form, cubic zinc blende (ZB) III-V NWs often adopt hexagonal wurtzite (WZ) phase or rotational twin layers resulting in polytypism (PT) between WZ and ZB structures. This phenomenon has been observed for most ZB compounds and epitaxial techniques, both for Au-assisted[6–9,13,21] and selective area[11] growth, also for III-V NWs deposited on (111)*B* (Refs. 6, 8, and 9) and Si (Refs. 13 and 21) substrates. Taking the example of GaAs, calculations give the difference in bulk cohesive energies ranging from 16.6 meV (Ref. 20) to 24 meV (Ref. 22) per III-V pair at zero ambient pressure. The value of 24 meV is indirectly supported by experimental results of Ref. 23. Cubic ZB phase becomes unstable at pressure higher than 14 GPa.[23] Experimental evidence strongly suggests that PT in ZB III-V NWs is somehow related to a small radius of NWs, resulting in a large relative contribution of lateral surfaces to the total free energy of fully formed NW, or monolayer islands mediating the

growth of the NW top. Despite the prevalence of WZ or PT structure in ZB III-V NWs, they often contain sequences of different phases and stacking faults. This clearly affects the material properties; so, the control over the phase purity is now considered as one of the main challenges in III-V NW fabrication.

Theoretical models of WZ and/or PT phase formation in ZB NWs proposed so far are the following. Models of Akiyama *et al.*[19,20] treat the structural stability by using calculations of cohesive energy as function of NW radius. Surface dangling bonds on the NW lateral facets are shown to have crucial effect to determine the stability. Since the number of dangling bonds is larger for ZB than for WZ phase, the formation of WZ NWs is favorable when surface energy gain is larger than the difference of volume cohesive energies. This leads to a certain critical radii of NWs, under which WZ phase should be predominant. Numerical estimates give the critical radius of 5.6 nm for GaAs (Ref. 20) and 6 nm for InP (Ref. 19) NWs, i.e., in order of magnitude smaller to explain the formation of WZ phase in NWs with radii up to at least 50 nm. Models[19,20] do not consider all PTs and study a fully formed single NW on a bare substrate. Model of Glas *et al.*[24] treats the free energy of formation of two-dimensional (2D) island in ZB or WZ position (orientation) from a supersaturated liquid alloy on the NW top. The authors show that 2D nucleation should take place at the edge of the liquid/solid interface (triple line) rather that at the center. If the island is formed at this triple line, the WZ nucleation is favored within a certain range of interfacial energies and at sufficiently high supersaturation of liquid alloy. This approach deals with the formation of only one monolayer in WZ position on top of ZB one, so nothing can be said about the resulting structure of fully formed NW (i.e., WZ or PT). In contrast to Refs. 19 and 20, the model of Ref. 24 is radius independent and applies only to the case of the VLS growth. Finally, simple estimation of the Laplace pressure $P=2\gamma_{L\text{-}V}/R$ in the Au-Ga liquid alloy with the liquid-vapor surface energy $\gamma_{L\text{-}V}$ between that of pure liquid Ga and Au [0.72 and 1.14 J/m^2 (Ref. 25)] equals 1.44–2.28 GPa for NW radius R as small as 1 nm. Therefore, the Laplace pressure in the drop is well below the transition from ZB to WZ or PT phase and cannot be considered as the effect entirely responsible for the latter.

This work addresses two aspects of NW formation discussed above. First, we present a very simple thermodynamic model of NW growth, treating the formation energy of an ensemble of identical NWs and a wetting layer between them from a vapor phase with given supersaturation. Within the framework of this model, we, however, take into consideration that the wetting layer and the NWs can form in different crystallographic phases than that of the substrate. We then compare the energies of different phases and morphological states of the system and draw some general conclusions concerning the NW formation mechanisms. In the second part of the work, we study the stability of different PTs between WZ and ZB, depending on the NW radius. Corresponding volume and surface energy terms are estimated simply by a linear scaling of bulk WZ-ZB energy difference[26] and by the number of dangling bonds on the lateral surface, respectively.[19,20] We consider PTs with the periods up to 18 monolayers and find the most energetically favorable phase. From this analysis, it is easy to construct phase diagrams describing the domains of radii and vapor supersaturations corresponding to the preferential formation of ZB NWs, PT NWs, and to unstable states with no NWs. Some numerical estimates for different III-V NWs are presented and analyzed.

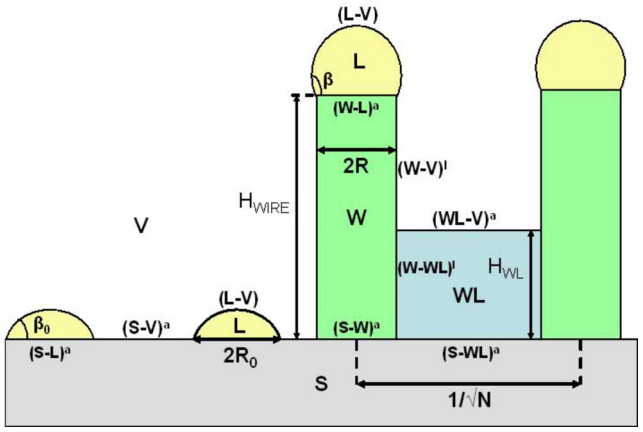

FIG. 1. (Color online) Schematics of NW formation showing the model parameters described in the text.

II. THERMODYNAMIC GROWTH MODEL

The model of NW formation is schematized in Fig. 1. We consider the most common case of NWs growing via the VLS mechanism,[17] although the further analysis is equally applicable to the case of VSS or catalyst-free growth. The initial state of the system consisting of the substrate, the drops, and the fixed amount of semiconductor material corresponds to a regular ensemble of N (1/m^2) spherical liquid drops per unit surface area with contact area with the substrate of radius R_0 and contact angle β_0 and volume H (m) of semiconductor material per unit surface area in the vapor phase (Fig. 1, left). The final state of the system is the regular ensemble of NWs grown perpendicular to the substrate, of same surface density N, radius R, and length H_{wire}, and a wetting layer of average thickness H_{WL} (Fig. 1, right), with drops of liquid alloy seated on top of NWs and having contact area of radius R and contact angle β with the top facet. NW is assumed as being a cylinder or a regular polygon; in the latter case, R is the radius of circle inscribed in the polygon. Since NWs and WL may form in different crystallographic phases, we generally consider five phases: vapor phase (V) with chemical potential μ_V, liquid phase (L) with chemical potential μ_L, and three solid phases of the substrate (S), NWs (W), and wetting layer (WL) with chemical potentials μ_S, μ_W, and μ_{WL}, respectively. Unless otherwise specified, all chemical potentials hereafter are referred to the unit volume (J/m^3). The surface energies (J/m^2) of interfacial boundaries, shown in Fig. 1, are denoted as follows: $\gamma^a_{S\text{-}W}$ for axial boundary $(S\text{-}W)^a$, $\gamma^a_{S\text{-}WL}$ for axial boundary $(S\text{-}WL)^a$, $\gamma^a_{WL\text{-}V}$ for axial boundary $(WL\text{-}V)^a$, $\gamma^l_{W\text{-}WL}$ for lateral boundary $(W\text{-}WL)^l$, $\gamma^l_{W\text{-}V}$ for lateral boundary $(W\text{-}V)^l$, $\gamma^a_{W\text{-}L}$ for axial

boundary $(W\text{-}L)^a$, $\gamma^a_{S\text{-}V}$ for axial boundary $(S\text{-}V)^a$, $\gamma^a_{S\text{-}L}$ for axial boundary $(S\text{-}L)^a$, and $\gamma_{L\text{-}V}$ for boundary $(L\text{-}V)$. Transition from the initial to the final state takes place due to the difference of chemical potentials in the vapor phase and in the substrate $\mu_V-\mu_S$, which is "switched on" at $t=0$ and "switched off" after the deposition of H monolayers onto the surface.

The volume contribution to free energy of the final state per unit surface area (J/m^2) equals the sum of volume energy accumulated in the NWs, in the wetting layer, and in the drops:

$$F_{volume} = N\pi R^2 H_{wire}\mu_W + (1 - N\pi R^2)H_{WL}\mu_{WL} + N\pi R^3 f(\beta)\mu_L. \quad (1)$$

Here, $f(\beta)$ is the function of the contact angle β that determines the drop volume. The surface energy contribution, accounting for all interfacial boundaries shown in Fig. 1, reads

$$F_{surface} = (1 - N\pi R^2)(\gamma^a_{S\text{-}WL} + \gamma^a_{WL\text{-}V}) + N\pi R^2\gamma^a_{S\text{-}W} + N2\pi RH_{WL}\gamma^{/}_{W\text{-}WL} + N2\pi R(H_{wire} - H_{WL})\gamma^{/}_{W\text{-}V} + N\pi R^2\gamma^a_{W\text{-}L} + N\pi R^2 g(\beta)\gamma_{L\text{-}V}. \quad (2)$$

Here, the first term stands for the surface energy between the NWs, changing due to the formation of a wetting layer, the second term describes the energy of axial boundary of NWs with the substrate surface, the third term relates to the lateral boundary of NWs with the wetting layer, the fourth term is the energy of lateral NW facets in contact with the vapor, the fifth term stands for the NW-liquid boundary, and the sixth for the liquid-vapor boundary. The function $g(\beta)$ describes the surface area of the drop in contact with the vapor. In Eqs. (1) and (2), we assume that $H_{wire} \geqslant H_{WL}$ so that the drops act as catalyst. The case of $H_{wire} < H_{WL}$, relating to the particles covered by wetting layer, is not considered here because the VLS growth in such conditions is not possible. Similar to Eqs. (1) and (2), the free energy of the initial state can be written as

$$F_0 = H\mu_V + N\pi R_0^3 f(\beta_0)\mu_L + (1 - N\pi R_0^2)\gamma^a_{S\text{-}V} + N\pi R_0^2\gamma^a_{S\text{-}L} + N\pi R_0^2 g(\beta_0)\gamma_{L\text{-}V}. \quad (3)$$

Here, the first two terms give the volume energy in the vapor and in the liquid phase, and the last three terms relate to the energy of the initial surface activated by catalyst drops. Equations (1)–(3) describe homogeneous crystallographic phases in NWs and WL and do not account for any of strain-induced contributions,[12,13] thus leaving aside the sequences of layers with different phases as well as the growth on the lattice-mismatched substrates.

Although it is not essential, we now assume that the drop volume remains approximately constant during the transition, yielding $R=R_0$ and $\beta=\beta_0$. In this case, all H monolayers of deposited material should be distributed in the NWs and the wetting layer, providing the mass conservation equation in the form

$$H = (1 - N\pi R^2)H_{WL} + N\pi R^2 H_{wire}. \quad (4)$$

In the following, we also neglect small changes in chemical potentials and surface energies which may occur due to variations in adatom and alloy concentrations during the growth. From Eqs. (1)–(4), we arrive at the following expression for the normalized difference in free energy of the final and the initial state (called hereafter formation energy), $\Delta f=(F-F_0)/[H(\mu_V-\mu_S)]$:

$$\Delta f = -1 + \frac{a + bz}{1 + z}. \quad (5)$$

Here,

$$z = \frac{\theta}{(1-\theta)}x \quad (6)$$

is the ratio of NW to wetting layer volume, $\theta=\pi R^2 N \ll 1$ is the fraction of surface covered by the drops, and $x=H_{wire}/H_{WL}$ is the ratio of NW length to the wetting layer thickness. For all reasonable N, the coverage θ is small, for instance, $\theta=0.028$ at $R=30$ nm and $N=10^9$ cm^{-2}. Obviously, x can range from 1 (2D growth with the drops overgrown by the wetting layer) to ∞ [three dimensional (3D) growth of NWs with an infinitely thin wetting layer], while z changes from $\theta/(1-\theta)$ at $x=1$ to ∞ at $x=\infty$ and finite θ. In Eq. (5), we do not write the terms proportional to R/H, since they vanish at $H \gg R$ and are not important for our further analysis. Coefficients of Eq. (5) contain chemical potentials of different phases and surface energies of lateral facets in the form

$$a = \frac{\mu_{WL} - \mu_S}{\mu_V - \mu_S} + \frac{\theta}{(1-\theta)}\frac{2(\gamma^{/}_{W\text{-}WL} - \gamma^{/}_{W\text{-}V})}{R(\mu_V - \mu_S)},$$

$$b = \frac{\mu_W - \mu_S}{\mu_V - \mu_S} + \frac{2\gamma^{/}_{W\text{-}V}}{R(\mu_V - \mu_S)}. \quad (7)$$

Volume contributions in Eq. (7) account for the difference of bulk cohesive energies in the wetting layer and the NWs. Surface energy contributions are inversely proportional to R and accounts for the Gibbs-Thomson effect of elevation of chemical potential in a NW of small radius, first modeled by Givargizov and Chernov[27] and subsequently studied in more detail in Refs. 14 and 16. R-dependent correction to free energy of NW ensemble is a macroscopic analog of corresponding results obtained for a single NW in Refs. 19 and 20.

Let us now consider coefficients a and b given by Eq. (7) in three general cases, without specifying particular crystallographic phases but assuming that the substrate phase has a lower chemical potential $(\mu_S \leqslant \mu_W)$ and a higher surface energy of lateral facets $(\gamma^{/}_{S\text{-}V} \geqslant \gamma^{/}_{W\text{-}V})$ than that of the NWs, as it happens in the case of ZB substrate and WZ NWs.[19,20]

Case 1. Crystallographic phases of substrate, WL, and NWs are identical $(W=WL=S)$. In this case, $\mu_W=\mu_{WL}=\mu_S$, $\gamma^{/}_{W\text{-}WL}=0$, and $\gamma^{/}_{W\text{-}V}=\gamma^{/}_{S\text{-}V}$, yielding

$$a_1 = -\frac{\theta}{1-\theta}b_1, \quad b_1 = \frac{2\gamma^{/}_{S\text{-}V}}{R(\mu_V - \mu_S)}. \quad (8)$$

Case 2. Crystallographic phase of NWs differs from the wetting layer, while the latter is the same as in the substrate ($W \neq WL = S$). We now have $\mu_W > \mu_{WL} = \mu_S$, $\gamma'_{W\text{-}WL} = \gamma'_{S\text{-}W}$, and Eqs. (7) are reduced to

$$a_2 = \frac{\theta}{(1-\theta)} \frac{2(\gamma'_{S\text{-}W} - \gamma'_{W\text{-}V})}{R(\mu_V - \mu_S)},$$

$$b_2 = \frac{1}{(\mu_V - \mu_S)} \left(\mu_W - \mu_S + \frac{2\gamma'_{W\text{-}V}}{R} \right). \quad (9)$$

Case 3. Crystallographic phases of NWs and wetting layer are identical but differ from that of the substrate ($W = WL \neq S$). In this case, $\mu_W = \mu_{WL} > \mu_S$, $\gamma'_{W\text{-}WL} = 0$, and Eqs. (7) give

$$a_3 = \frac{1}{(\mu_V - \mu_S)} \left(\mu_W - \mu_S - \frac{\theta}{(1-\theta)} \frac{2\gamma'_{W\text{-}V}}{R} \right), \quad b_3 = b_2. \quad (10)$$

For all three cases considered, the function Δf defined in Eq. (5) increases with z. This follows from $\Delta f(z=0) = -1 + a$, $\Delta f(z=\infty) = -1 + b$, and $b - a \propto \mu_W - \mu_{WL} + 2(\gamma'_{W\text{-}V} - \theta\gamma'_{W\text{-}WL})/[R(1-\theta)] > 0$ at $\mu_W \geqslant \mu_{WL}$ and small θ. Global minimum of free energy is reached at $z = \theta/(1-\theta)$ and $x = 1$, corresponding to 2D surface layer with no NWs. Therefore, all NW ensembles observed should be considered as metastable and essentially kinetically controlled, because the formation of NW lateral surface is thermodynamically unfavorable. Due to a growth inhibition by chemical or physical catalyst discussed in the Introduction, metastable states with $x > 1$ exist within a finite period of time but must decay under an infinite exposition. This implies that the value of x is itself controlled by the growth kinetics. From the experimental evidence,[5,28] we know that NW growth rate is usually much higher than that of wetting layer, so that x increases with the growth duration, ideally from 1 to ∞. Within the framework of our model, metastable NW arrays relate to $\Delta f < 0$, which means that growth thermodynamics favors the crystallization of semiconductor material from the vapor phase. The states with $\Delta f > 0$ should be considered as thermodynamically forbidden, and all semiconductor materials must remain in the vapor phase.

We now analyze the domains of metastable and thermodynamically forbidden states and compare free energies of different phase configurations in the metastable region. Considering, for simplicity, an idealized case of $x = z = \infty$, pure 3D NW growth is possible at $\Delta f(\infty) = -1 + b < 0$, yielding the lower limit for radius R of the form

$$R > R_{min} = \frac{2\gamma'_{W\text{-}V}}{\mu_V - \mu_W}. \quad (11)$$

In case 1 of identical crystallographic phases, Eq. (11) transforms into the known Givargizov-Chernov formula $R_{min} = R_{GC} = 2\gamma'_{S\text{-}V}/(\mu_V - \mu_S)$.[27] Equation (11) gives the generalized nonequilibrium restriction for NW radius, since it contains vapor chemical potential μ_V related to the material flux. The NWs would not grow from the drops with radii $R < R_{min}$, because the vapor supersaturation is insufficient to overcome the Gibbs-Thomson effect.[14] Further, case 3 for any x requires higher formation energy compared to case 2, because $b_3 = b_2$ and $a_3 > a_2$. Hence, wetting layer should always adopt the structure of the substrate. To study possible scenarios of crystallographic phases, we now need to compare Δf_1 and Δf_2 in cases 1 and 2 at $z = \infty$. Equation (5) shows that at $b_1 < b_2$, the NWs would tend to adopt the structure of the substrate, while at $b_1 > b_2$, the situation is reverse and the NWs would grow in a different phase. From Eqs. (8) and (9), this leads to the critical radius of crystallographic phase transition with the new phase emerging at

$$R < R_c = \frac{2(\gamma'_{S\text{-}V} - \gamma'_{W\text{-}V})}{\mu_W - \mu_S}. \quad (12)$$

In contrast to Eq. (11), this condition is only material related. Whenever Eq. (12) is satisfied, NWs would adopt a new crystallographic phase at x exceeding a certain critical value x_c. Since $a_1 < a_2$, NWs of small length would always grow in the substrate phase. Combining conditions of Eqs. (11) and (12), the NW growth is forbidden at $R < R_{min}$, and the NWs tend to adopt a crystallographic structure different from that of the substrate at $R_{min} < R < R_c$ and tend to grow in the substrate phase at $R > R_c$. These general conclusions are insufficient, however, to predict actual NW structure as well as to estimate the values of R_{min} and R_c. The aim of the next section is the analysis of energetically favorable PTs in ZB III-V NWs, based on thermodynamic considerations described above.

III. POLYTYPISM IN III-V NANOWIRES

We now study the case of a ZB III-V (111)*B* (As-terminated) substrate ($\mu_S = \mu_{ZB}, \gamma'_{S\text{-}V} = \gamma'_{ZB}$) and PT NWs ($\mu_W = \mu_{PT}, \gamma'_{W\text{-}V} = \gamma'_{PT}$), growing perpendicular to the substrate. In the case of ZB wires, the lateral surface is formed by {1100} facets, while WZ NWs can have either {1100} or {11−20} facets along the growth direction. These facets have the same total number of dangling bonds, with As and Ga atoms containing two dangling bonds, so that the both facets are identical within the framework of our simplified model. For further analysis, it is convenient to introduce the hexagonality α, the normalized surface energy of the PT τ, and the characteristic radius R_0 by the definitions:

$$\alpha = \psi_{PT}/\psi_{WZ}, \quad \tau = \gamma'_{PT}/\gamma'_{ZB}, \quad R_0 = \gamma'_{ZB}/\psi_{WZ}. \quad (13)$$

Here, for brevity, $\psi_{WZ} = \mu_{WZ} - \mu_{ZB}$ is the difference of chemical potentials between the bulk WZ and ZB phases and $\psi_{PT} = \mu_{PT} - \mu_{ZB}$ is the same difference between the bulk PT and ZB phases. Our definitions yield $\alpha \leqslant 1$ and $\tau \leqslant 1$. For illustrative clearness, in Fig. 2 we present the crystal structures of ZB and WZ phases. Since the values of γ'_{ZB} and ψ_{WZ} are fixed and more or less known,[29] the quantity R_0 characterizes particular material system, e.g., $R_0 = 17$–25 nm for GaAs [at $\psi_{WZ} = 16.6$–24 meV/Ω,[20,22] $\gamma'_{ZB} = \gamma^{(110)}_{ZB} = 1.5$ J/m^2, and the volume per GaAs pair in the crystal $\Omega = 0.045$ nm^3 (Ref. 29)]. Using standard notation for the difference of chemical potentials in the vapor and ZB phases, $\Delta\mu = \mu_V - \mu_{ZB}$, Eqs. (11) and (12) can be rewritten in the form

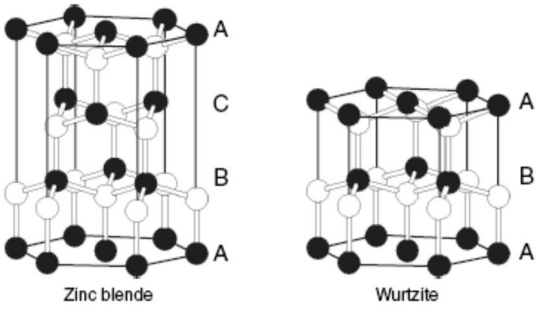

FIG. 2. Crystal structure of ZB (left) and WZ (right) phases showing their $ABCABC\cdots$ and $ABAB\cdots$ stacking sequences.

$$R_{min} = \frac{2\tau}{(\Delta\mu/\psi_{WZ} - \alpha)} R_0, \quad R_c = \frac{2(1-\tau)}{\alpha} R_0. \tag{14}$$

Formation energy of PT NW ensemble at $z=\infty$ $\Delta f_2(\infty) = -1 + b_2$ now equals

$$\Delta f_2(\infty) = -1 + \frac{\psi_{WZ}}{\Delta\mu}\left(\alpha + 2\tau\frac{R_0}{R}\right). \tag{15}$$

Table I summarizes the known PTs between WZ and ZB structures[26,29] with the period up to 18 monolayers. In column 1, we present the standard notations for different PTs, where the number gives the lattice periodicity and the letter denotes the symmetry group. Column 3 describes the standard stacking sequence in the growth direction in terms of atom positions, and column 4 presents the same sequence in terms of hexagonal WZ (h) and cubic ZB (c) positions (orientations) of particular layers. The Zhdanov symbols[26] given in column 2 are readily obtained from the layer sequence as the number of WZ layer in the sequence, e.g., (22)=*chch* for 4*H* PT. Hexagonality of the PT α, given in column 5, is obtained from column 4 simply as the fraction of WZ layers in the total number of layers, e.g., $\alpha=2/4=0.5$ for 4*H* PT. Assuming that the coefficient α in the first equation of Eqs. (13) is the same as the hexagonality of the PT in Table I, we adopt the linear scaling of ψ_{PT} with the fraction of WZ layers, which seems feasible. In order to estimate the surface energy τ for different PTs, we simply count the number of dangling bonds j on the lateral facets. This procedure is illustrated in Fig. 3 in the case of WZ, ZB, and 4*H* PT structures. The results for j are given in column 6 of Table I. We then assume that the surface energy is proportional to the

TABLE I. Polytypes between wurtzite and zinc blende structures. Bold rows relate to PTs with maximum critical radius of ZB-WZ transition.

PT	Zhdanov symbol	Stacking sequence	Layer sequence	α	j	τ
2*H*	(1 1)	*AB*	*hh*	1.000	1.000	0.750
3*C*	**∞**	***ABC***	***ccc***	**0.000**	**1.333**	**1.000**
4*H*	**(2 2)**	***ABAC***	***chch***	**0.500**	**1.000**	**0.750**
6*H*	(3 3)	*ABCBAC*	*cchcch*	0.333	1.333	1.000
8*H*	(4 4)	*ABCACBAC*	*ccchccch*	0.250	1.250	0.938
8*L*	(7 1)	*ABCABCAC*	*ccccccch*	0.250	1.250	0.938
10*L*	**(8 2)**	***ABCABCABAC***	***cccccchch***	**0.200**	**1.200**	**0.900**
10*L*	(3 3 2 2)	*ABCBACABAC*	*cchcchchch*	0.400	1.200	0.900
10*H*	**(5 5)**	***ABCABACBAC***	***ccchccccch***	**0.200**	**1.200**	**0.900**
12*R*	(3 1)^3	*ABCBCABABCAC*	*cchhcchhcchhcchh*	0.500	1.333	1.000
12*H*	(6 6)	*ABCABCBACBAC*	*cccchccccch*	0.167	1.333	1.000
12*L*	(9 3)	*ABCABCABCBAC*	*ccccccchcch*	0.167	1.333	1.000
12*L*	(4 4 2 2)	*ABCACBACABAC*	*ccchccchchch*	0.333	1.167	0.875
14*H*	(7 7)	*ABCABCACBACBAC*	*cccccchcccccch*	0.143	1.286	0.964
14*L*	(13 1)	*ABCABCABCABCAC*	*ccccccccccchh*	0.143	1.286	0.964
14*L*	(5 4 2 3)	*ABCABACBABCBAC*	*ccchccchchcch*	0.286	1.286	0.964
14*L*	(5 5 1 1 1 1)	*ABCABACBACACAC*	*ccchcccchhhhh*	0.429	1.143	0.857
14*L*	(5 3 1 1 1 3)	*ABCABACBCBCBAC*	*ccchchchhhhcch*	0.429	1.286	0.964
14*L*	**(5 5 2 2)**	***ABCABACBACABAC***	***ccchccchchch***	**0.286**	**1.143**	**0.857**
14*L*	(4 4 3 3)	*ABCACBACABCBAC*	*ccchccchcchcch*	0.286	1.286	0.964
14*L*	(3 3 3 3 1 1)	*ABCBACABCBACAC*	*cchcchchcchhh*	0.429	1.286	0.964
16*H*	**(8 8)**	***ABCABCABCBACBACB***	***cccccchccccccch***	**0.125**	**1.250**	**0.938**
16*L*	**(14 2)**	***ABCABCABCABCABAC***	***ccccccccccchch***	**0.125**	**1.250**	**0.938**
16*L*	(5 5 3 3)	*ABCABACBACABCBAC*	*ccchccchchchcch*	0.250	1.250	0.938
16*L*	(3 3 3 3 2 2)	*ABCBACABCBACABAC*	*cchcchchchchchch*	0.375	1.250	0.938
18*R*	(4 2)*3	*ABCACBCABCBABCABAC*	*ccchchccchchccchch*	0.333	1.333	1.000

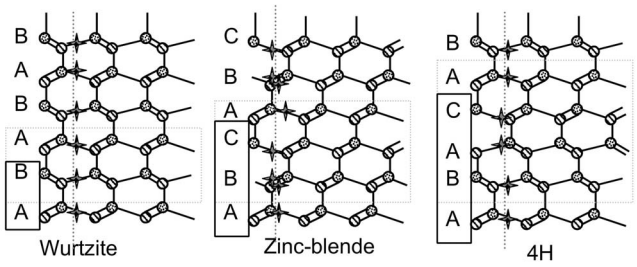

FIG. 3. Side view of WZ, ZB, and 4*H* PT structures. Star symbols indicate the dangling bonds on the lateral facet. The number of dangling bonds j in the WZ phase equals 1 per layer in the WZ and 4*H* PT phases and 4/3 in the ZB phase.

number of dangling bonds and calculate $\tau(j)=3j/4$, presented in column 7 of Table I.

Figure 4 presents graphically the results of Table I in (α,τ) plane. From the second equation of Eqs. (14), it follows that the maximum radius of ZB to PT phase transition is reached at maximum value of $2(1-\tau)/\alpha$. For all PTs considered, this expression is not larger than 1 and equals 1 for four structural types: 4*H*, 10*H* (10*L*), 14*L*, and 16*H* (16*L*) (for pairs 10*H*, 10*L* and 16*H*, 16*L*, coefficients α and τ are identical). Corresponding (α,τ) coordinates are placed on the straight line shown in Fig. 4. These PTs are bold in Table I, together with pure ZB 3*C* phase, also placed on the line $\tau=1-\alpha/2$. For these PTs, $R_c=R_0$, while for all other PTs, $R_c<R_0$, in particular, $R_c=R_0/2$ for pure WZ (8.5–12.5 nm for GaAs). To find the most energetically favorable crystallographic phase within the range $R_{min}R<R_c$, we compare the formation energies given by Eq. (15) for all PTs with maximum $R_c=R_0$, for which $\Delta f_2(\infty)=-1+2(\psi_{WZ}R_0/\Delta\mu R)-(\psi_{WZ}/\Delta\mu)(R_0/R-1)\alpha$. This equation shows that the minimum formation energy relates to maximum α, i.e., in the case of 4*H* PT. The differences of formation energies of all PTs with $R_c=R_0$ and of ZB structure in meV ($\Delta F_{PT}=\Omega\Delta\mu\Delta f_2$) as functions of NW radius are presented in Fig. 5, where the corresponding curve for WZ structure is shown for reference. It is seen that the curves for all PTs intersect at $R=R_0$, relating to $\Delta F_{PT}=\Delta F_{ZB}$. In the PT range $R<R_c$, 4*H* PT has the lowest energy, which is also

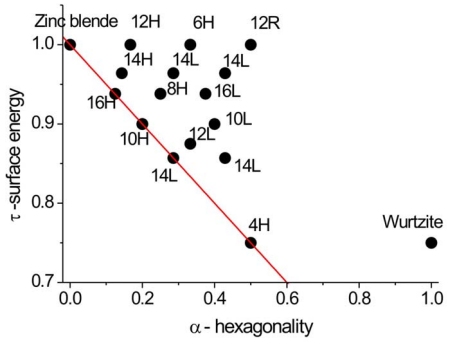

FIG. 4. (Color online) (α,τ) coordinates of different PTs between WZ and ZB. Points on the straight line $\tau=1-\alpha/2$ relate to the maximum critical radius of ZB to PT transition $R_c=R_0$.

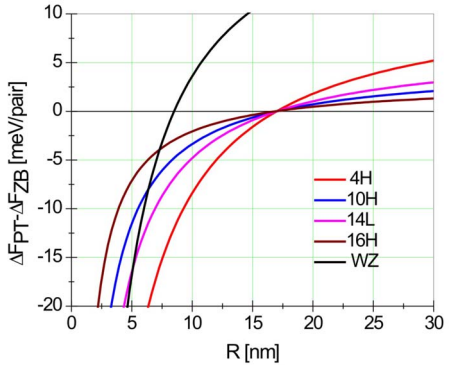

FIG. 5. (Color online) Difference $\Delta F_{PT}-\Delta F_{ZB}$ for 4*H*, 10*H*, 14*L*, and 16*H* PTs and WZ structure at $\psi_{WZ}=24$ meV, $\Delta\mu=287$ meV, and $R_0=17$ nm. The value of $\Delta\mu$ corresponds to MBE growth of GaAs on the GaAs(111)*B* substrate at $T=580$ °C and nominal growth rate=0.2 nm/s (Ref. 30).

lower than that of pure WZ structure and of all other PTs presented in Table I. Therefore, 4*H* PT should be considered as the most thermodynamically favorable PT structure of ZB NWs.

As mentioned already, the critical radius R_c, under which PT structure is prevalent, is only material related, while the minimum radius R_{min} of NW formation is a kinetic value decreasing at higher vapor supersaturation. This is illustrated by the phase diagram for ZB-4*H* PT transition in the $(\Delta\mu,R)$ plane in Fig. 6, where we plot $\Delta\mu$-independent $R_c=17$ nm and two curves of $R_{min}(\Delta\mu)$ for ZB and 4*H* PT structures. These lines divide the whole plane into three regions relating to the formation of ZB NWs, 4*H* PT NWs, and no NWs. At $R<R_c$, 4*H* PT NWs can only grow above the curve 2. Therefore, the formation of PT NWs requires not only small radius but also sufficiently high vapor supersaturation.

Similar kinetic condition follows from the model of Glas *et al.*,[24] which is, however, obtained from completely different considerations and applies to the supersaturation of liquid phase during the VLS growth. During MBE growth of GaAs NWs on the GaAs(111)*B* substrate with nominal growth rate of 0.2 nm/s, the values of $\Delta\mu$ range approximately from

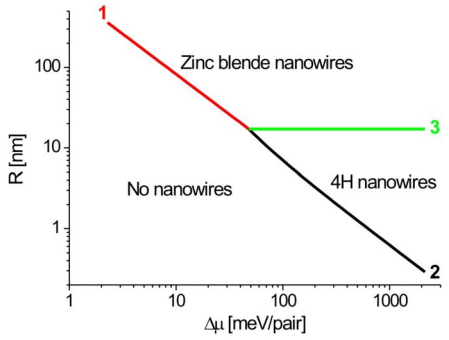

FIG. 6. (Color online) R-$\Delta\mu$ phase diagram of ZB-4*H* PT transition in GaAs NWs ($R_c=17-25$ nm) obtained from Eqs. (14): $1-R_{min}$ for ZB phase, $2-R_{min}$ for 4*H* PT phase, and $3-R_c=17$ nm.

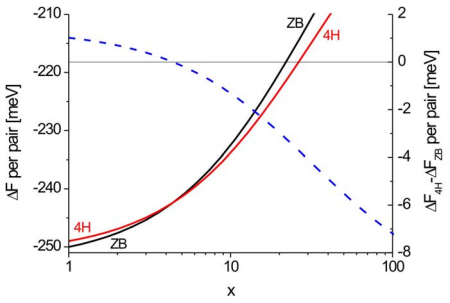

FIG. 7. (Color online) Graphs showing the ZB to 4*H* PT transition at increasing the NW length. Curves $\Delta F(x)=\Delta F_{PT}=\Omega\Delta\mu\Delta f(x)$ are obtained from Eqs. (5)–(7) at $\psi_{ZB}=24$ meV, $\gamma^{1}_{ZB}=1.5$ J/m^2, $\theta=0.03$, and $R=10$ nm for ZB and 4*H* structures.

250 to 450 meV at typical growth temperatures $T=500-600$ °C, with smaller values of $\Delta\mu$ relating to higher T.[24,30] This provides the estimate for R_{min} from 1.41 to 2.62 nm, i.e., much smaller than R_c. For the parameters of Fig. 5, minimum radii equal 2.23 nm for 4*H* PT, 2.60 nm for 10H PT, 2.50 nm for 14L PT, 2.69 nm for 16H PT, and 2.33 nm for WZ structure.

Conditions for PT formation given by Eqs. (14) apply only to the case of $z=x=\infty$. In real growth experiment, at least in MBE technique, we always observe the formation of wetting layer of a finite thickness.[5] Figure 7 demonstrates that the ZB-PT structural transformation takes place only at a certain critical x_c. As discussed earlier, the value of x should generally increase with the growth time, so sufficiently short NWs adopt the ZB phase and longer NWs are PTs. This conclusion qualitatively confirms with the experimental observations in the case of MBE growth of GaAs NWs on the GaAs(111)*B* substrate.[6,24]

It is noteworthy that the presented approach applies to all ZB III-V NWs, regardless of rather crude assumptions made in estimations of α and τ for different PTs. The only material-related parameter in Eqs. (14) for R_{min} and R_c is the characteristic radius R_0. More accurate calculations of α and τ would affect the numerical values of R_{min} and R_c and consequently the phase diagrams, but the general picture of NW formation and structural phase transitions remains qualitatively as described. Table II summarizes the values of R_0 estimated by means of the last equation of Eqs. (13) for different ZB III-V materials. We use the data of Ref. 31 for (110) surface energies of ZB crystals; the differences of chemical potentials between WZ and ZB phase are taken from Ref. 20. It is seen that R_0 is of order of several tens of nanometers for all materials considered. As discussed earlier, hexagonal phase becomes prevalent at $R=R_0$ for 4*H* PT and at $R=R_0/2$ for pure WZ phase. Phosphides are characterized by the highest, arsenides by intermediate, and antimonides by the lowest radii of transition.

Finally, in our simplified model, it is assumed that the lateral surfaces are strictly parallel to the growth direction. While this should always hold for a WZ NW, it can be shown that the lateral surface of a cubic crystal, growing perpendicular to the (111) surface, may exhibit periodic sawtooth faceting.[32] Such oscillatory behavior of NW radius may be observed in VLS growth, at least at near-equilibrium conditions, because the cubic NW has no stable orientation parallel to the (110) growth direction and has been already observed experimentally for Si NWs grown on the Si(111) substrates.[28,32] This effect would lead to the increase of effective area of NW lateral surface in contact with the vapor for the ZB phase. Corresponding increase in the surface energy would reduce the value of τ in Eqs. (14) and increase the critical radius for the crystallographic phase transformation.

IV. CONCLUSIONS

The presented model allows us to draw several general conclusions concerning the NW formation in different epitaxial techniques. First, all NW ensembles should be treated as metastable and kinetically controlled, because the formation of their sidewalls is thermodynamically unfavorable. Due to the Gibbs-Thomson effect, the NWs would not grow at all if the growth seed is smaller than a certain minimum radius R_{min}. The value of R_{min} depends on the crystallographic structure of NWs. Above R_{min}, the NWs adopt PT structure at R smaller than critical radius R_c and ZB structure for larger R. The formation of PTs in III-V ZB NWs is qualitatively explained by the decrease of surface energy of lateral

TABLE II. Characteristic radius of transition from ZB to WZ phase in III-V NWs.

Material	Elementary volume Ω (nm^3)	(110) surface energy γ^{1}_{ZB} (J/m^2)	Difference of cohesive energies ψ_0 (meV/pair)	Characteristic radius R_0 (nm)
AlAs	0.0451	1.8	16.4	30.9
AlP	0.0398	2.4	11.4	52.4
AlSb	0.0567	1.3	19.0	24.3
GaAs	0.0451	1.5	16.6	25.5
GaP	0.040	2	11.6	43.6
GaSb	0.0567	1.1	19.8	19.7
InAs	0.0567	1	10.6	33.5
InP	0.0506	1.3	6.8	60.4
InSb	0.068	0.75	16.4	19.4

facets, which outweighs the increase of bulk cohesive energy at sufficiently small R.[19,20] Therefore, the formation of PTs in ZB NWs generally requires two conditions: small enough radius of the NW and high enough supersaturation of the vapor phase. Analysis of hexagonality and surface energy gain for different PTs between WZ and ZB structure shows that $4H$ PT has the lowest formation energy and should be considered as the one controlling the NW structure from thermodynamic viewpoint. Wetting layer between the NWs should always grow in ZB phase. The transition from ZB to PT structure occurs at a certain critical length of the NWs so that shorter NWs always form in ZB phase. Our numerical estimates provide the value of $R_c=17-25$ nm for GaAs NWs. Due to thermal fluctuations, one can expect the observation of WZ layers even above R_c as well as transitions between ZB, different PTs, and pure WZ structure. The model can be applied to all III-V ZB NWs grown on the lattice matched $(111)B$ substrates. However, more accurate calculations of coefficients α and τ for different PTs are required. It should be noted that our model treats only the thermodynamics of fully formed, phase homogeneous NWs and therefore cannot describe the sequences of different structures. We also neglect all kinetic growth effects, in particular, 2D nucleation,[24] which can strongly influence the resulting structure. While it is shown that the NW formation is controlled by the growth process rather than by thermodynamics, it is particularly important to consider the kinetics of WZ layer formation as well as the effect of the position of the preceding layer on the formation of the next one. Finally, the model can be generalized to account for the growth on the lattice-mismatched substrates, e.g., of III-V NWs on Si(111), by taking into consideration strain-induced renormalizations of volume and surface energies.

ACKNOWLEDGMENTS

This work was partially supported by the Russian Federal Agency for Science and Innovation (Contract No. 02.513.11.3042), SANDIE Network of Excellence of European Commission, and different grants of the Russian Academy of Sciences and Russian Foundation for Basic Research. We thank F. Glas, J. C. Harmand, G. E. Cirlin, and I. P. Soshnikov for many stimulating discussions.

*dubrovskii@mail.ioffe.ru

[1] T. Bryllert, L.-E. Wernersson, L. E. Froberg, and L. Samuelson, IEEE Electron Device Lett. **27**, 323 (2006).
[2] F. Qian, Y. Li, S. Gradecak, D. Wang, C. J. Barrelet, and C. M. Lieber, Nano Lett. **4**, 1975 (2004).
[3] E. Patolsky, G. Zheng, O. Hayden, M. Lakadamyali, X. Zhuang, and C. M. Lieber, Proc. Natl. Acad. Sci. U.S.A. **101**, 14017 (2004).
[4] K. A. Dick, K. Deppert, T. Mårtensson, B. Mandl, L. Samuelson, and W. Seifert, Nano Lett. **5**, 761 (2005).
[5] V. G. Dubrovskii, G. E. Cirlin, I. P. Soshnikov, A. A. Tonkikh, N. V. Sibirev, Yu. B. Samsonenko, and V. M. Ustinov, Phys. Rev. B **71**, 205325 (2005).
[6] J. C. Harmand, G. Patriarche, N. Péré-Laperne, M.-N. Mérat-Combes, L. Travers, and F. Glas, Appl. Phys. Lett. **87**, 203101 (2005).
[7] M. Koguchi, H. Kakibayashi, M. Yasawa, K. Hiruma, and T. Katsuyama, Jpn. J. Appl. Phys., Part 1 **31**, 2061 (1992).
[8] A. I. Persson, M. W. Larsson, S. Stenstrom, B. J. Ohlsson, L. Samuelson, and L. R. Wallenberg, Nat. Mater. **3**, 678 (2004).
[9] I. P. Soshnikov, G. E. Cirlin, A. A. Tonkikh, Y. B. Samsonenko, V. G. Dubrovskii, V. M. Ustinov, O. M. Gorbenko, D. Litvinov, and D. Gerthsen, Phys. Solid State **47**, 2213 (2005).
[10] J. Noborisaka, J. Motohisa, and T. Fukui, Appl. Phys. Lett. **86**, 213102 (2005).
[11] P. Mohan, J. Motohisa, and T. Fukui, Nanotechnology **16**, 2903 (2005).
[12] F. Glas, Phys. Rev. B **74**, 121302(R) (2006).
[13] L. C. Chuang, M. Moewe, S. Crankshaw, C. Chase, N. P. Kobayashi, and C. Chang-Hasnain, Appl. Phys. Lett. **90**, 043115 (2007).
[14] V. G. Dubrovskii and N. V. Sibirev, Phys. Rev. E **70**, 031604 (2004).
[15] A. I. Persson, L. E. Fröberg, S. Jeppesen, M. T. Björk, and L. Samuelson, J. Appl. Phys. **101**, 034313 (2007).
[16] V. G. Dubrovskii, N. V. Sibirev, G. E. Cirlin, J. C. Harmand, and V. M. Ustinov, Phys. Rev. E **73**, 021603 (2006).
[17] R. S. Wagner and W. C. Ellis, Appl. Phys. Lett. **4**, 89 (1964).
[18] S. A. Kukushkin and A. V. Osipov, Prog. Surf. Sci. **51**, 1 (1996).
[19] T. Akiyama, K. Nakamura, and T. Ito, Phys. Rev. B **73**, 235308 (2006).
[20] T. Akiyama, K. Sano, K. Nakamura, and T. Ito, Jpn. J. Appl. Phys., Part 2 **45**, L275 (2006).
[21] I. P. Soshnikov, G. E. Cirlin, A. A. Tonkikh, V. V. Nevedomskii, Yu. B. Samsonenko, and V. M. Ustinov, Phys. Solid State **49**, 1440 (2007).
[22] C.-Y. Yeh, Z. W. Lu, S. Froyen, and A. Zunger, Phys. Rev. B **46**, 10086 (1992).
[23] M. I. McMahon and R. J. Nelmes, Phys. Rev. Lett. **95**, 215505 (2005).
[24] F. Glas, J. C. Harmand, and G. Patriarche, Phys. Rev. Lett. **99**, 146101 (2007).
[25] A. Zangwill, *Physics at Surfaces* (Cambridge University Press, Cambridge, 1988).
[26] I. T. Steinberger, Prog. Cryst. Growth Charact. **7**, 7 (1983).
[27] E. I. Givargizov and A. A. Chernov, Kristallografiya **18**, 147 (1973).
[28] L. Schubert, P. Werner, N. D. Zakharov, G. Gerth, F. M. Kolb, L. Long, U. Gösele, and T. Y. Tan, Appl. Phys. Lett. **84**, 4968 (2004).
[29] *Group IV Elements, IV-IV and III-V Compounds*, edited by U. Rössler, Landolt-Börnstein, New Series, Group III, Vol. 41, Part A (Springer, Berlin, 2006).
[30] V. G. Dubrovskii, N. V. Sibirev, R. A. Suris, G. E. Cirlin, J. C. Harmand, and V. M. Ustinov, Surf. Sci. **601**, 4395 (2007).
[31] J. W. Cahn and R. E. Hanneman, Surf. Sci. **1**, 38 (1964).
[32] F. M. Ross, J. Tersoff, and M. C. Reuter, Phys. Rev. Lett. **95**, 146104 (2005).